J. Plasma Physics (2001), *vol.* 65, *part* 5, *pp.* 353–363. © 2001 Cambridge University Press
DOI: 10.1017/S0022377801001131 Printed in the United Kingdom

Relativistic electron heating in laser-produced plasmas

LIHUA CAO,[1,2] TIEQIANG CHANG,[3] WENWEI CHANG[1] and ZONGWU YUE[1]

[1]Applied Physics Department, National University of Defense Technology, Changsha Hunan, 410073, P. R. China

[2]Laboratory of Computational Physics, Institute of Applied Physics and Computational Mathematics, PO Box 8009, Beijing 100088, P. R. China

[3]Institute of Applied Physics and Computational Mathematics, PO Box 8009, Beijing 100088, P. R. China

(Received 16 August 1999 and in revised form 20 January 2000)

Abstract. Two-dimensional multi-timescale fully electromagnetic relativistic particle simulation is used to investigate relativistic electron heating in laser-produced plasmas. When laser pulses with peak intensities $10^{19}\,\mathrm{W\,cm^{-2}}$ and different durations (e.g. 118 fs and 442 fs) are incident on overdense plasma slabs with step-like density profiles, the dynamics of plasmas and Fourier frequency spectra from our particle simulations demonstrate distinctly different properties in hot-electron temperatures, absorption, relativistic electron heating, and so on. The particular motions of the critical surfaces are discussed. From the two examples simulated in this paper, it is concluded that the interactions between plasmas and laser pulses with the same intensities and different durations are dominated by different mechanisms, which can lead to dissimilar dynamics of plasmas, relativistic heating, and so on.

1. Introduction

The recent advent of compact high-intensity subpicosecond lasers with chirped pulse amplification (CPA) has opened up a new field of study of laser-matter interaction [1, 2], and has a wide range of applications, such as the X-ray lasers [3–6], laser fusion [7–9] laser-plasma accelerators [10–17], harmonic generation in plasmas and gases [18–20], and laser-plasma channeling [21–23]. The study of the absorption and electron acceleration of high-intensity laser pulses incident on a target surface is of great interest. This subject has been studied extensively, both experimentally and theoretically. Some new and complicated physical phenomena appear, and the underlying physics is strongly nonlinear. The super-intense laser pulses are extremely short; for example, it is the short pulse duration that makes particle-in-cell (PIC) simulations of relativistic laser–plasma interaction feasible. As pointed out by Pukhov and Meyer-ter-Vehn [24], two-dimensional PIC simulations have already become a 'workhorse' in studies of relativistic laser plasma interaction [25], and three-dimensional PIC simulations of actual experiments have now been reported [24, 26].

The absorption of intense laser in plasmas is a basic problem; the laser can interact with the plasma by a variety of processes. In particular, collective processes

https://doi.org/10.1017/S0022377801001131 Published online by Cambridge University Press

are important for such intense laser light ($I\lambda^2 > 10^{17}\,\mathrm{W}\,\mu\mathrm{m}^2\,\mathrm{cm}^{-2}$, where I is the intensity of the laser and λ is its wavelength); its absorption depends on plasma density, plasma scale length, laser polarization, and angle of incidence. In such a laser intensity, the oscillating electron motion becomes relativistic, and some new physical phenomena arise. Some novel mechanisms, such as the so-called 'not-so-resonant' resonant absorption of Brunel [27, 28], the anomalous skin effect [29, 30], and $\mathbf{J} \times \mathbf{B}$ heating [31–33] have been proposed to explain the absorption processes.

The effects of a prepulse have been investigated experimentally [34–35] by varying the temporal separation between the main laser pulse and a prepulse, so plasmas with different lengths and density gradients are produced. It is found that the temperature of high-energy electrons depends strongly on the preformed plasma produced by the prepulse. However, the influences of relativistic effects and the ponderomotive force as well as the incident pulse shape on the plasma dynamics are not well understood.

In this paper, we attempt to investigate absorption and relativistic electron heating in plasmas produced by laser pulses with the same peak intensities $10^{19}\,\mathrm{W\,cm}^{-2}$ but different durations. The two-dimensional, multi-timescale, fully electromagnetic, and relativistic particle-in-cell (PIC) code (LPI2D), which has been used successfully to study resonant absorption and some physical mechanisms [36–40], will be used to investigate the problem. The dynamics of the plasmas and the analysis of the Fourier frequency spectrum from our simulations indicate that there are different mechanisms of absorption and relativistic electron heating for different durations of laser pulses, which create plasmas with different scale lengths and gradients. By comparison of the computer results, the essential features of relativistic electron heating and absorption are explored.

2. Computer-simulation set-up

The PIC method is based on fundamental equations for the particles and electromagnetic fields, and provides a very detailed kinetic description of plasmas [41, 42]. The evolution of electromagnetic fields and the relativistic motions of particles are described respectively by the Maxwell equations and the Lorentz equation.

In two-dimensional particle simulation, the particles move in the (x, y) plane, and there are three components of the electromagnetic field, E_x, E_y, and B_z. A multi-timescale algorithm is introduced in order to reduce computational cost [42, 43]. The evolution of electromagnetic fields and the motion of ions and electrons are advanced in different time steps, i.e. $\Delta t_e, = \Delta t, \Delta t_i = N\,\Delta t$, $\Delta t_E = 0.5\,\Delta t, 0.5\,\Delta t, \Delta t_B = 0.25\,\Delta t, 0.5\,\Delta t, 0.25\,\Delta t$ where $\Delta t_e, \Delta t_i, \Delta t_E$, and Δt_B devote respectively the time steps of advancing electrons, ions, the electric field, and the magnetic field. The numerical experiments demonstrate that the algorithm can describe correctly the behavior of plasmas, and greatly enhances the computational efficiency [43].

An intense, linear polarized laser light beam with Gaussian time behavior $I = I_0 \exp[(t - t_0)^2/2\tau^2]$ is launched normally from the left-hand boundary onto an overdense plasma slab with density $4n_c$, where n_c, is the critical density above which the laser cannot propagate and t_0 is chosen as 2τ. The electric field is in the plane of motion of particles (i.e. the (x, y) plane). The wavelength λ of the laser light is assumed to be $1.06\,\mu\mathrm{m}$. In this paper, the peak intensity of the laser I_0 is assumed to be $10^{19}\,\mathrm{W\,cm}^{-2}$, τ is chosen as 50 fs and 188 fs (the corresponding full width at half maximum (FWHM) of the laser pulse is respectively 118 fs and 442 fs and the

https://doi.org/10.1017/S0022377801001131 Published online by Cambridge University Press

laser pulse reaches its peak intensity at time $\omega_0 t \approx 178$ and $\omega_0 t \approx 668$, where ω_0 is the frequency of the laser light). Our simulations can be run well beyond the peak of the pulse.

Initially, electrons and ions are laid down on a two-dimensional grid and constitute a definite plasma with density $4n_c$. The system is 5λ long and 2.5λ wide, and is divided into a 256×128 grid. Initial velocities both for electrons and ions have have Maxwellian distributions with temperature of 1 keV for electrons and $\frac{1}{3}$ keV for ions. The ion–electron mass ratio is assumed to be 1836, and the ions are pushed once every 20 time steps [43]. About 200 000 electrons and 200 000 ions are followed in the self-consistent electromagnetic fields.

3. Simulation results and discussion

For different laser durations, the plasmas have different scale lengths and density gradients, so the electron acceleration mechanisms are dissimilar. In order to discern the characters of heating, just as in most PIC codes, the distributions of the particles in phase space and the energy spectra of electrons, as well as the density profiles of ions or electrons, are recorded. In our simulation, the position of the critical surface is also memorized during the calculations. First, the density profile in the x-direction can be achieved in every step; the position of the critical surface is calculated by judging and interpolation.

In addition, in PIC simulations, the effective temperature of electrons can be evaluated approximately by the slope of the energy spectrum [44]. So multiple-temperature phenomena are observed directly from it. Absorption is calculated in the usual way from the time-averaged Poynting vector at the left-hand boundary, and from the rate of increase of energy of particles leaving the right-hand boundary. An analysis of the Fourier frequency spectrum is also performed when discussing the mechanisms of relativistic electron heating.

Two examples with the same wavelengths ($1.06\,\mu$m) and peak intensity ($10^{19}\,\mathrm{W\,cm^{-2}}$) but different durations (118 fs FWHM and 442 fs FWHM, corresponding for $\tau = 50$ fs and $\tau = 187.5$ fs) will be exhibited as follows. In the following exposition, all the figure parts (*a*) and (*b*) correspond respectively to the results of laser pulses with duration of 118 fs and 442 fs.

For a 118 fs laser pulse, the plasma has almost no time to expand during the duration of the laser pulse, so that the scale length of the plasma formed by it is small. This situation is similar to that discussed previously [39]. In the non-relativistic limit, an electromagnetic wave cannot propagate in the plasma where the electron density is higher than the critical density. But for a relativistic intense laser, the electron in the laser field oscillates with great quiver velocity, which is of the order of the speed of light, the relativistic effect increases the electron mass and decreases the effective plasma frequency, and self-induced transparency (SIT) [45] enables the laser to penetrate deeply into the supercritical density plasma and propagate beyond the critical density. Meanwhile, the relativistic effect still results in a great ponderomotive force.

The longitudinal electric field and the electron distribution in phase space (x, P_x), at $\omega_0 t = 173.6$ are illustrated in Fig. 1(a). It is clear that groups of energetic electrons in the overdense plasma zone are generated and are separated by roughly half of the laser wavelength. Those electrons are evidently accelerated by the $\mathbf{J} \times \mathbf{B}$ force, which dominates the mechanism of $\mathbf{J} \times \mathbf{B}$ heating [31–33, 39]. The so-called

https://doi.org/10.1017/S0022377801001131 Published online by Cambridge University Press

$\mathbf{J}\times\mathbf{B}$ heating is caused by the electrostatic field driven by the oscillating component of the ponderomotive force, which has two components oscillating with frequencies 0 and $2\omega_0$ for linear polarized laser light [31]. The electrons are driven into the overdense plasma due to the huge ponderomotive force, so a positive electrostatic field is set up near the interface. At the same time, the electron density profile is also modulated crudely by a frequency $2\omega_0$ as shown in Fig. 2(a). Apparently, the structures of field and the longitudinal density profile coincide with the locations of accelerated particles.

The diagnostics of the Fourier frequency spectrum is carried out by recording the evolutions of electromagnetic fields. Figure 3(a) is the Fourier frequency spectrum for the longitudinal electric field at a determinate special position $(\frac{1}{2}L_x, \frac{1}{2}L_y)$. The longitudinal electric field E_x has principally $0, \omega_0$ and $2\omega_0$ components; the zero and second harmonics are more intense. The second harmonic is generated in the longitudinal direction; it is caused by the $\mathbf{V}\times\mathbf{B}/c$ force, which has components 0 and $2\omega_0$ for a linearly polarized laser light. It is agreement with Kruer's and Estabrook's predication of $\mathbf{J}\times\mathbf{B}$ heating [31].

If the laser duration is changed to 442 fs, a great difference will appear. Figure 1(b) is a snapshot of the longitudinal and electron distributions in phase space (x, P_x); the corresponding electron density profile at the same moment is illustrated in Fig. 2(b). They are different from those in Figs 1(a) and 2(a). At that moment, the laser intensity is rising and has not reached its peak intensity; the ponderomotive force is not so large that $\mathbf{J}\times\mathbf{B}$ heating has not been responsible for the process of laser plasma interaction. The electrons at the vacuum–plasma interface are pushed into the vacuum by the thermal pressure, so a negative electrostatic field is produced to maintain quasineutrality at the interface, as shown in Fig. 1(b). At the same time, numerous fast electrons are created mainly in the forward direction in the longitudinal direction, but they do not obviously depart by a distance of half a wavelength in the (P_x, x) plot. The features of $2\omega_0$ modulation disappear. Figure 3 is a snapshot of the electron distribution in phase space (x, P_x) and the corresponding electron density profile at $\omega_0 t = 694.20$ when the laser intensity is near its peak ($\omega_0 t \approx 668$). Since the underdense plasma region, due to expansion of the plasma, allows the electromagnetic wave to propagate in it, the electrons in the underdense plasma may be heated by a variety of instabilities.

If a Fourier analysis of the frequency spectrum is also carried out, it is found that there is a considerable difference from the shorter laser pulse described above. For a pulse duration of 118 fs, at a spatial position $(\frac{1}{2}L_x, \frac{1}{2}L_y)$, the longitudinal electric field has a $2\omega_0$ component (Fig. 4a), which results from $\mathbf{J}\times\mathbf{B}$ heating. But for a pulse duration of 442 fs, there is only a ω_0 component, as shown in Fig. 4(b), and there are no second or higher harmonics generated. The density gradient may also prevent efficient harmonic generation. Furthermore, the electron distributions in phase space and the results from the Fourier frequency spectra lead to the same conclusion.

The great pressure near the vacuum–plasma interface due to the huge ponderomotive force pushes on the overdense plasma, generating a shock propagating into the overdense plasma region and creating spike-like density profiles. The evolution of ion density profiles (Fig. 5b) exhibits a density peak up to $16.5n_c \approx 4$ times the background density when the laser pulse is near its peak intensity. This high-density region may apparently influence the relativistic transparency; even if the initial electron density is in a transparent regime, the density may be increased locally over the threshold value above which the laser pulse cannot propagate.

https://doi.org/10.1017/S0022377801001131 Published online by Cambridge University Press

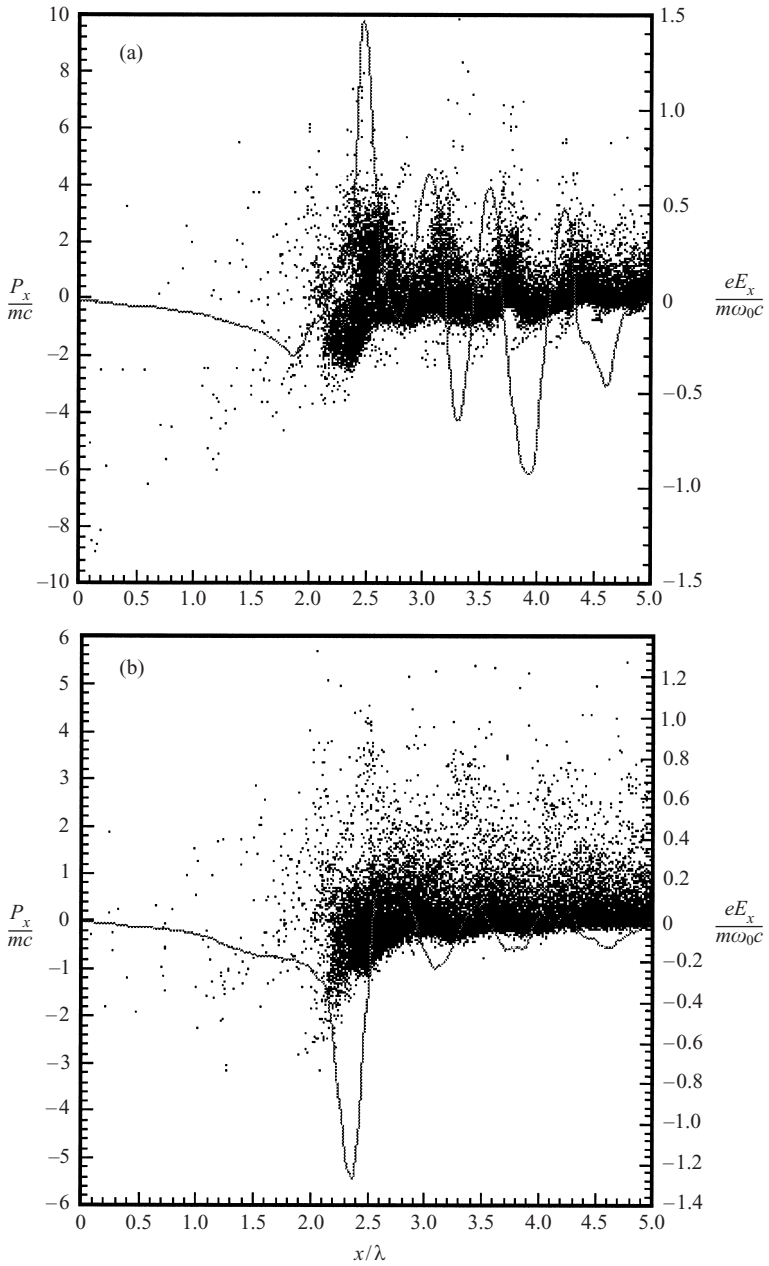


Figure 1. The longitudinal electric field and electrons in phase space (x, P_x) at $\omega_0 t = 173.6$: (*a*) pulse duration 118 fs; (b) pulse duration 442 fs.

The Doppler shift of light reflected from the critical surface can be crudely estimated as $\Delta\lambda/\lambda = -2(v_{\rm exp}/c)\cos\theta$, where $v_{\rm exp}$ is the expansion velocity of the critical surface, θ is the angle of incidence and c is the speed of light in vacuum. Competition between ponderomotive and thermal forces can result in a red- or blueshift in frequency of the reflected light [46]. It is found that when the average electron quiver energy becomes comparable to the electron thermal energy,

https://doi.org/10.1017/S0022377801001131 Published online by Cambridge University Press

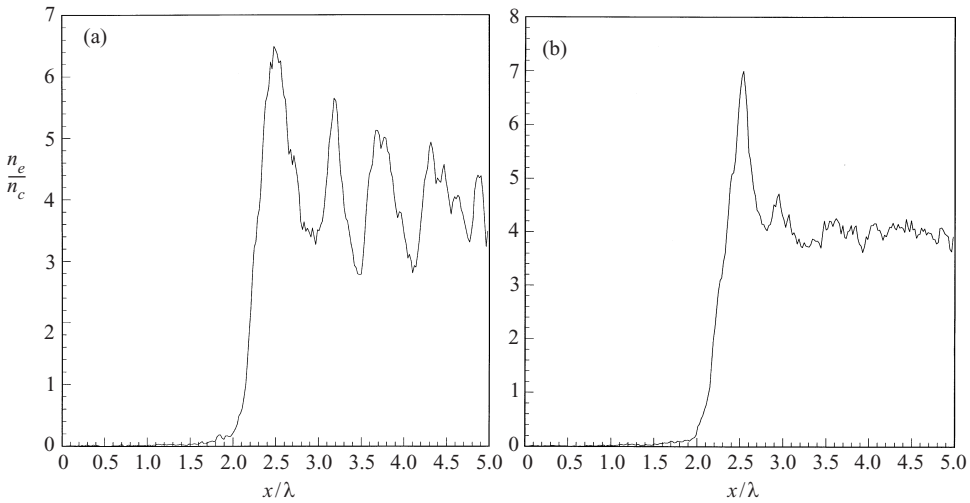


Figure 2. The electron density profile at $\omega_0 t = 173.6$: (a) pulse duration 118 fs; (b) pulse duration 442 fs.

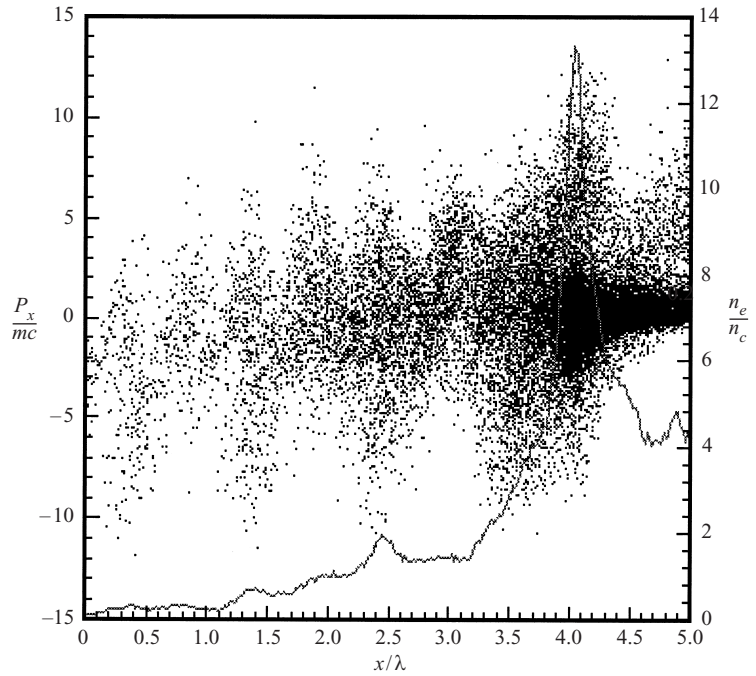


Figure 3. The electron distribution in phase space (x, P_x) and the corresponding electron density profile at $\omega_0 t = 694.2$.

the ponderomotive force of the high-intensity laser significantly reduces the laser plasma thermal expansion. In the conditions considered here, the critical surface moves toward the overdense plasma at a velocity of about $0.009c$, and its direction does not alter during our calculations. It can be inferred that the Doppler shift to the red is about 0.018. In fact, experiments carried out with lower-intensity lasers

https://doi.org/10.1017/S0022377801001131 Published online by Cambridge University Press

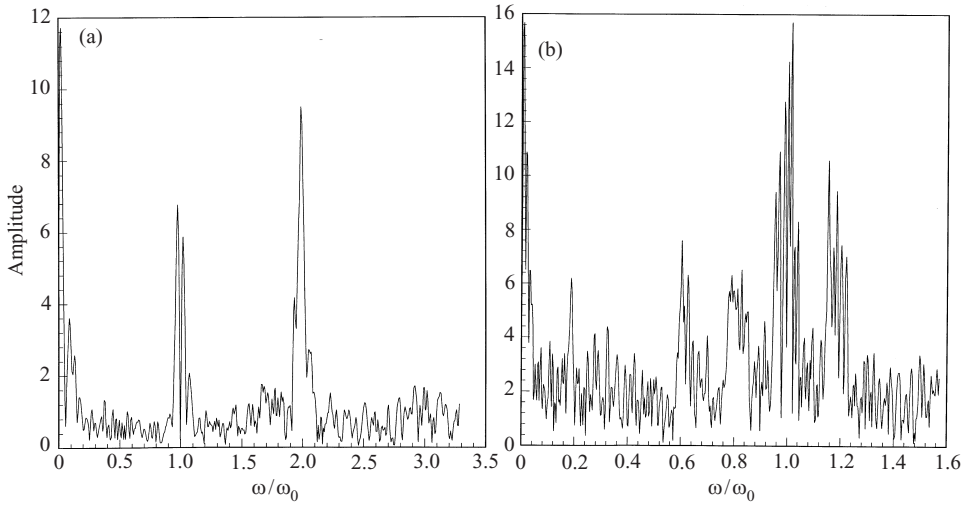


Figure 4. The Fourier spectrum of the longitudinal electric field at the spatial point $(\frac{1}{2}L_x, \frac{1}{2}L_y)$: (a) pulse duration 118 fs; (b) pulse duration 442 fs.

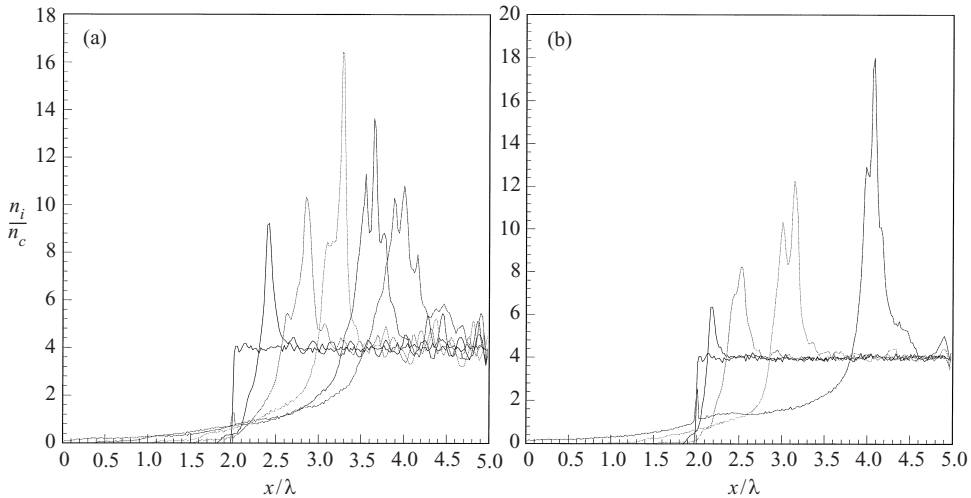


Figure 5. Ion density profiles at different moments: (a) $\omega_0 t$ = 0, 173.6, 260.3, 347.1, 433.9 and 520.7; (b) $\omega_0 t$ = 0, 173.6, 347.1, 520.7 and 694.2.

(e.g. $I\lambda^2 = 10^{15}\,\mathrm{W}\,\mu\mathrm{m}^2\,\mathrm{cm}^{-2}$) have already observed a reduction in the expected blueshift of the reflected light due to ponderomotive effects at the critical surface [46]. The evolution of the position of the critical surface can be diagnosed in detail in particle simulations as shown in Fig. 6(b).

In $\mathbf{J} \times \mathbf{B}$ heating, the electron temperature is dominated by the ponderomotive potential. An estimate of the electron temperature on strong irradiation, particularly when the deposition takes place in a localized region near n_c, is given by E_p, the ponderomotive energy of the electrons oscillating in the laser field [47]:

$$E_p = 0.511 \left[\left(1 + \frac{I\lambda^2}{1.4 \times 10^{18}} \right)^{1/2} - 1 \right] \mathrm{MeV}.$$

https://doi.org/10.1017/S0022377801001131 Published online by Cambridge University Press

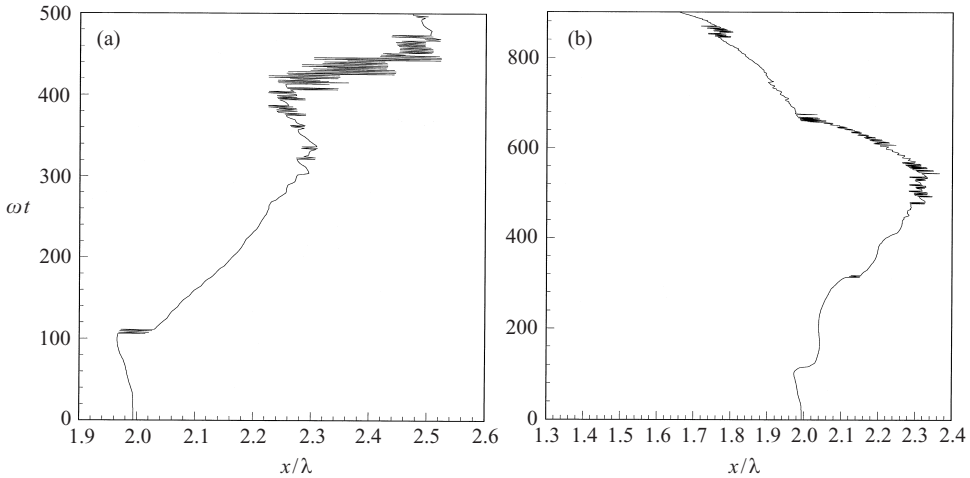


Figure 6. Time dependence of the position of the critical surface where $n_i = n_c$.

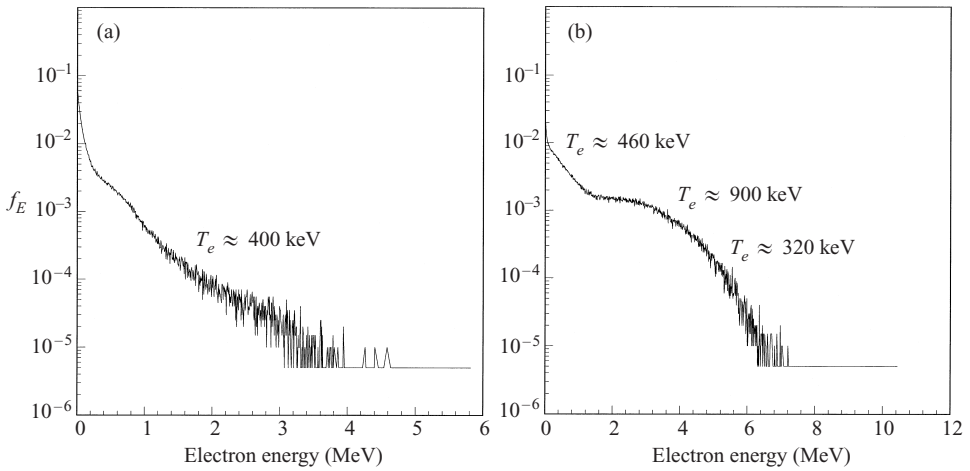


Figure 7. Electron energy spectrum at (a) $\omega_0 t = 173.6$ and (b) $\omega_0 t = 694.2$.

If the intensity of laser pulse remains constant, as discussed in [29], the temperature of hot electrons remains in agreement with the ponderomotive energy. But under the conditions considered here, the laser has a time-dependent pulse shape, which is taken to be Gaussian. If the ponderomotive energy is estimated as above, assuming $\lambda = 1.06\,\mathrm{m}$, then $E_p \approx 1\,\mathrm{MeV}$, for $I = 10^{19}\,\mathrm{W\,cm^{-2}}$ and $E_p \approx 0.63\,\mathrm{MeV}$ for $I = 0.5 \times 10^{19}\,\mathrm{W\,cm^{-2}}$. Figure 7(a) shows the electron energy spectrum at $\omega_0 t = 173.6$, which is composed of a relatively cold main body plus a quasi-Maxwellian heated tail with a temperature of about 400 keV; generation of hot electrons is observed.

A 442 fs laser pulse will reach its peak intensity after a longer time, so the plasma has some time to expand and has a longer scale length; this may result in some differences. The ion density profiles at different moments $\omega_0 t = 0, 173.6, 347.1, 520.6$ and 694.2 are exhibited in Fig. 5(b). Plasma expands toward to vacuum, and a shock

https://doi.org/10.1017/S0022377801001131 Published online by Cambridge University Press

wave propagating into overdense plasma is generated simultaneously with the rising laser intensity and the corresponding increase in the ponderomotive force.

It should be mentioned here that the critical surface moves towards the overdense plasma zone before $\omega_0 t \approx 560$ and then moves in the opposite direction. At the turning moment, the laser has even not reached its peak intensity, but the electrons has been heated to be so much that the thermal force becomes comparable to the huge ponderomotive force. The particular motion of the critical density surface is the result of competition between ponderomotive and thermal forces [46]. The peculiar motion of the critical surface is confirmed by our computer simulations, as illustrated in Fig. 6(b).

In fact, the complicated motion of the critical density surface is investigated experimentally by observing the red- and blueshifts of a backscattered fundamental wave [48]. The experimental results indicates that the critical density surface moves either towards the overdense plasma region or in the opposite direction, depending on the steepness of the pulse front. When the laser pulse is clean and the plasma gradient is steep, the critical density moves only in the direction of the plasma corona. This is similar to the case for the 118 fs FWHM laser pulse.

In the early stage, electrons have not been accelerated adequately by the laser, so the electron thermal energy is smaller than the average electron quiver energy, so the ponderomotive force effect prevails over thermal expansion, and a Doppler shift to the red occurs. With rising laser intensity, some suprathermal electrons with very high temperature are produced, the plasma thermal expansion overwhelms the ponderomotive force and a Doppler shift to the blue emerges. The electron energy spectrum at $\omega_0 t = 694.2$ is shown in Fig. 7(b). It demonstrates that several groups of electrons with multiple temperatures are born in the process of laser plasma interactions. Some energetic electrons have temperature ranging up to 900 keV which is close to the ponderomotive energy, and those suprathermal electrons do not reach the tail of the energy spectrum.

Finally, it is necessary to demonstrate the conservation of energy in our simulations. All the energies are recorded and taken into account; they include the kinetic energies of ions and electrons, the energies of electro-magnetic fields and the difference of kinetic energy of those 'escaped particles' that escape the boundaries. The time dependence of the relative error in the check of energy conservation is shown in Fig. 8. It can be observed that the relative error is limited to 10% at the beginning, and then fluctuates between 2% and 0.2% for most of the time of the calculation. So energy conservation is well satisfied in the simulations.

4. Conclusions

Computer simulations of relativistic electron heating and absorption may go some way to explaining the differences in the temperatures of the heated electrons and the absorption at the same laser intensity but with different laser pulse durations. With the help of two-dimensional PIC simulations, we have characterized the basic features of relativistic electron heating and the absorption. The electron distributions in phase space, the patterns of electric fields, the evolution of ion density profiles and multiple temperature phenomena have been presented and discussed. In particular, the motion of the critical density surface has been determined and compared with the experimental results. A Fourier analysis has been carried out and reasonable results obtained

https://doi.org/10.1017/S0022377801001131 Published online by Cambridge University Press

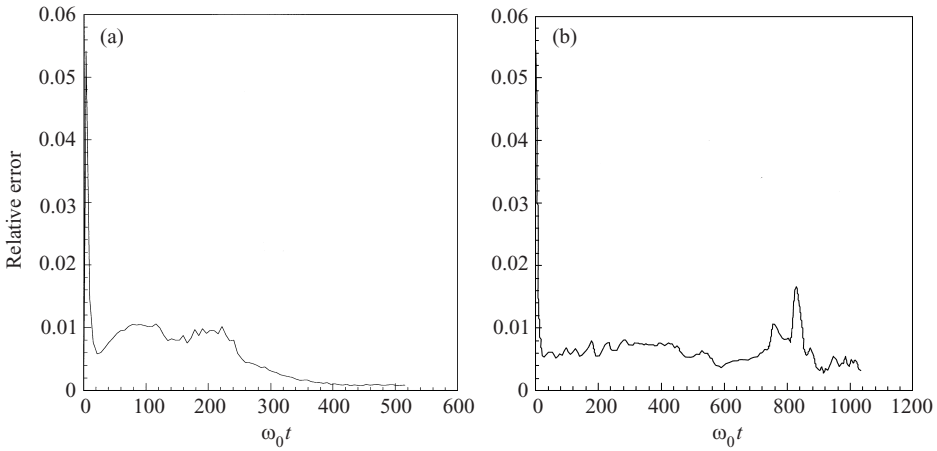


Figure 8. The time dependence of the relative error in the check of energy conservation: (a) pulse duration 118 fs; (b) pulse duration 442 fs.

Acknowledgements

We gratefully acknowledge the support of the National High Technology ICF Committee in China, the Youth Science Fund of the National High Technology ICF Committee in China, the National Natural Science Fund of China and the National Postdoctoral Science Fund of China.

References

[1] Perry, M. D. and Mourou, G., *Science* **264**, 917 (1994).
[2] Mourou, G. and Umstadter, D., *Phys. Fluids* **B4**, 2315 (1992).
[3] Suckewer, S. and Skinner, C. H., *Science* **247**, 1553 (1990).
[4] Eder, D. C., Amendt, P., Dasilva, L. B., London, R. A., MacGowan, B. J., Matthews, P. L. et al., *Phys. Plasmas* **1**, 1744 (1994).
[5] Lemoff, B. E., Yin, G. Y., Gordan, C. L. III, Barty, C. P. J. and Harris, S. E., *Phys. Rev. Lett.* **74**, 1574 (1995).
[6] Eisenberger, P. and Suckewer, S., *Science* **274**, 201 (1996).
[7] Tabak, M., Hammer, J., Ginsky, M. E., Kruer, W. L., Wilks, S. C., Woodworth, J. et al., *Phys. Plasmas* **1**, 626 (1994).
[8] Delamater, N. D., Marphy, T. J., Haner, A. A., Kaufman, R. L., Richard, A. L., Lindman, E. L. et al., *Phys. Plasmas* **3**, 2022 (1996).
[9] Pawley, C. J., Gerber, K., Lehmberg, R. H., Melean, E. A., Mostovych, A. N., Obenschain, S. P. et al., *Phys Plasmas* **4**, 1969 (1997).
[10] Sprangle, P., Esarey, E., Ting, A. and Joyce, G., *Appl. Phys. Lett.* **53**, 2146 (1988).
[11] Sprangle, P., Esarey, E. and Ting, A., *Phys. Rev. Lett.* **64**, 2011 (1990)
[12] Sprangle, P., Esarey, E., Krall, J. and Joyce, G., *Phys. Rev. Lett.* **69**, 2200 (1992).
[13] Esarey, E., Sprangle, P., Krall, J. and Ting, A., *IEEE Trans. Plasma Sci.* PS-24, 252 (1997).
[14] Clayton, C. E., Everett, M. J., Lal, A., Gorden, D., Marsh, K. A. and Joshi, C., *Phys. Plasmas* **1**, 1753 (1994).
[15] Modena, A., Najmudin, Z., Dangor, A. E., Clayton, C. E., Marsh, K. A., Joshi, C. et al., *Nature* **377**, 606 (1995)
[16] Umstadter, D., Chen, S.-Y., Maksimchuk, A., Mourou, G. and Wagner, R., *Science* **273**, 472 (1996).

https://doi.org/10.1017/S0022377801001131 Published online by Cambridge University Press

[17] Ting, A., Moore, C. I., Krushelnick, K., Manka, C., Esarey, E., Sprangle, P. et al., *Phys. Plasmas* **4**, 1899 (1997).
[18] Macklin J., Kmetec, J. and Gordon, C., *Phys. Rev. Lett.* **7**, 760 (1993).
[19] Sprangle, P. and Esarey, E., *Phys. Rev. Lett.* **67**, 2021 (1991).
[20] Esarey, E., Ting, A., Sprangle, P., Umstadter, D. and Liu, X., *IEEE Trans. Plasma Sci.* **21**, 95 (1993).
[21] Milchberg, H. M., Clark, T. R., Durfee, C. G. III, and Antonsen, T. M., *Phys. Plasmas* **3**, 2149 (1996).
[22] Ehrlich, Y., Cohen, C., Zigler, A., Krall, J., Sprangle, P. and Esarey, E., *Phys. Rev. Lett.* **77**, 4186 (1996).
[23] Sprangle, P., Esarey, E. and Krall, J., *Phys. Rev.* **E54**, 4211 (1996).
[24] Pukhov, A. and Meyer-ter-Vehn, J., *Phys. Plasmas* **5**, 1880 (1998).
[25] Dawson, J., *Phys. Plasmas* **2**, 2189 (1995).
[26] Borghesi, M., MacKinnon, A. J., Barringer, L., Gaillard, R., Gizzi, L. A., Meyer, C. et al., *Phys. Rev. Lett.* **78**, 879 (1997).
[27] Brunel, F., *Phys. Rev. Lett.* **59**, 52 (1987).
[28] Gibbon, P. and Bell, A. R., *Phys. Rev. Lett.* **68**, 1535 (1992).
[29] Rozmous, W. and Tikonshuk, V. T., *Phys. Rev.* **A42**, 7401 (1990).
[30] Gamaliy, E. G. and Dragila, R., *Phys. Rev.* **A42**, 929 (1990).
[31] Kruer, W. L. and Estabrook, K., *Phys. Fluids* **28**, 430 (1985).
[32] Wilks, S. C., *Phys. Fluids* **B5**, 2603 (1993).
[33] Denavit, J., *Phys. Rev. Lett.* **69**, 3052 (1992).
[34] Zhang, P., He, J. T., Chen, D. B., Li, Z. H., Zhang, Y., Bian, J. G. et al., *Phys. Rev.* **E57**, 3746 (1998).
[35] Bastiani, S., Rousse, A., Geindre, J. P., Audebert, P., Auoix, C. and Hamoniaux, G., *Phys. Rev.* **E56**, 7179 (1997).
[36] Cao, L., Chang, W. and Yue, Z., *Phys. Plasmas* **5**, 499 (1998).
[37] Cao, L., Chang, W., Yue, Z. and Zhao, Y., *Chinese J. Lasers* **24**, 947 (1997) (in Chinese).
[38] Cao, L., Chang, W., Yue, Z. and Zhao, Y., *High Power Laser and Particle Beams* **9**, 178 (1997) (in Chinese).
[39] Cao, L., Chang, T., Chang, W. and Yue, Z., *High Power and Particle Beams* **10**, 80 (1998) (in Chinese).
[40] Cao, L., Chang, T., Chang, W. and Yue, Z., *High Power and Particle Beams* **10**, 433 (1998) (in Chinese).
[41] Dawson, J. M., *Rev. Mod. Phys.* **55**, 403 (1983).
[42] Birdsall, K. and Longdon, A. B., *Plasma Physics via Computer Simulation*. New York: McGraw-Hill, 1985.
[43] Cao, L., Liu, D., Chang, W. and Yue, Z., *J. Natl Univ. Defense Technol.* **18**, 133 (1996) (in Chinese).
[44] Degroot, J. S. and Tull, J. E., *Phys. Fluids* **18**, 672 (1975).
[45] Fuchs, J., Adam, J. C., Amiranoff, F., Baton, S. D., Gallant, P. and Gremillet, L., *Phys. Rev. Lett.* **80**, 2326 (1998).
[46] Liu, X. and Umstadter, D., *Phys. Rev. Lett.* **69**, 1935 (1992).
[47] Campbell, E. M., *Phys. Fluids* **B4**, 3781 (1992).
[48] Kalashnikov, M. P., Nickles, P. V., Schlegel, Th., Schnuerer, M., Billhardt, F., Will, I. et al., *Phys. Rev. Lett.* **73**, 260 (1994).

https://doi.org/10.1017/S0022377801001131 Published online by Cambridge University Press